AIP Journal of Applied Physics

Investigation of the mechanism of impurity assisted nanoripple formation on Si induced by low energy ion beam erosion

Sarathlal Koyiloth Vayalil, Ajay Gupta, Stephan V. Roth, and V. Ganesan

Citation: Journal of Applied Physics **117**, 024309 (2015); doi: 10.1063/1.4905684
View online: http://dx.doi.org/10.1063/1.4905684
View Table of Contents: http://scitation.aip.org/content/aip/journal/jap/117/2?ver=pdfcov
Published by the AIP Publishing

Articles you may be interested in

Nanopatterning of metal-coated silicon surfaces via ion beam irradiation: Real time x-ray studies reveal the effect of silicide bonding
J. Appl. Phys. **113**, 124305 (2013); 10.1063/1.4797480

Real time x-ray studies during nanostructure formation on silicon via low energy ion beam irradiation using ultrathin iron films
Appl. Phys. Lett. **101**, 263104 (2012); 10.1063/1.4773202

Sharp transition from ripple patterns to a flat surface for ion beam erosion of Si with simultaneous co-deposition of iron
AIP Advances **2**, 032123 (2012); 10.1063/1.4739843

Nanopatterning of Si surfaces by normal incident ion erosion: Influence of iron incorporation on surface morphology evolution
J. Appl. Phys. **109**, 104315 (2011); 10.1063/1.3585796

Highly ordered self-organized dot patterns on Si surfaces by low-energy ion-beam erosion
Appl. Phys. Lett. **87**, 033113 (2005); 10.1063/1.2000342

[This article is copyrighted as indicated in the article. Reuse of AIP content is subject to the terms at: http://scitation.aip.org/termsconditions. Downloaded to] IP: 131.169.95.181 On: Thu, 22 Jan 2015 12:46:14

JOURNAL OF APPLIED PHYSICS **117**, 024309 (2015)

Investigation of the mechanism of impurity assisted nanoripple formation on Si induced by low energy ion beam erosion

Sarathlal Koyiloth Vayalil,[1,2,a)] Ajay Gupta,[3] Stephan V. Roth,[1] and V. Ganesan[2]
[1]*Photon Science, DESY, Notkestr. 85, D-22607 Hamburg, Germany*
[2]*UGC-DAE Consortium for Scientific Research, University Campus, Khandwa Road, Indore 452017, India*
[3]*Amity Center for Spintronic Materials, Amity University, Sector 125, Noida 201313, India*

(Received 20 August 2014; accepted 28 December 2014; published online 13 January 2015)

A detailed mechanism of the nanoripple pattern formation on Si substrates generated by the simultaneous incorporation of pure Fe impurities at low energy (1 keV) ion beam erosion has been studied. To understand and clarify the mechanism of the pattern formation, a comparative analysis of the samples prepared for various ion fluence values using two complimentary methods for nanostructure analysis, atomic force microscopy, and grazing incidence small angle x-ray scattering has been done. We observed that phase separation of the metal silicide formed during the erosion does not precede the ripple formation. It rather concurrently develops along with the ripple structure. Our work is able to differentiate among various models existing in the literature and provides an insight into the mechanism of pattern formation under ion beam erosion with impurity incorporation. © *2015 AIP Publishing LLC*. [http://dx.doi.org/10.1063/1.4905684]

I. INTRODUCTION

Recently, there has been a huge interest in the studies of nanostructure formation on semiconductors via low energy ion beam irradiation.[1–8] It is found to be an efficient technique to grow nanostructures in a single step over a large area. These nanostructured surfaces are found to be useful to act as a template to grow thin films and multilayers to tailor functional properties in controlled manner.[9–17] In general, ripple like structures are found to be formed, when a flat surface of any elemental solid is bombarded with ions at oblique angle of incidence. Bradley and Harper have given the first satisfactory theoretical explanation by considering the competition between surface instability caused by the curvature dependent sputtering and surface relaxation mechanism, so called B-H model.[18] Following that, many refined theoretical models have been derived to predict experimentally observed features during the formation of regular patterns.[19–23] Ripple formation during oblique angle irradiation on technologically important Si surfaces has begun in large magnitude by the studies of Carter and Vishnyakov.[24,25]

Furthermore, nanodot formation study by Gago *et al.*[26] on Si surfaces under normal incidence has generated a new view on pattern formation at the nano scale. Ozaydin *et al.*[27] observed that the surface remains flat at normal incidence ion bombardment under ultra-high vaccum condition which was contradicting the observation of Gago *et al.*[26] These observations strongly suggest that the nanopattern observed in earlier experimental reports on Si surface was due to the unintentionally deposited impurities. Madi *et al.*[28] demonstrated a phase diagram which shows no pattern formation at the normal incidence. The study of formation of disordered arrays of nanodots during the normal incidence ion beam sputtering with the addition of a trace amount of Molybdenum by Ozaydin *et al.*[29] led to a wealth of experimental and theoretical developments on the importance of impurities during ion beam sputtering on nanopattern formation.

Macko *et al.*[30] studied the off-normal incidence ion sputtering of Si with Fe co-deposition. Hofsäss *et al.* reported that simultaneous incorporation of different metal ions, such as Au, Ag, and Pt "surfactants" during ion beam sputtering leads to novel surface nanopatterns on Si surfaces.[31] A transition from hole to dot patterns on Si by tuning the amount of metal incorporation during ion sputtering at normal incidence has been observed by Sánchez-García *et al.*[32] There are some theoretical models for the observed ion beam induced patterns due to the simultaneous deposition of impurities or in binary compounds. Recently, Shenoy *et al.*[33] proposed a model to describe sputtering of alloy surfaces, which describes the evolution of both surface height and composition. Bradley and Shipman[34] reconsidered the B-H model for binary compounds and for concurrent deposition of impurities during sputtering. The importance of coupling between surface height and composition in the nanodot pattern formation has been described. Zhang *et al.*[35] did a detailed study of surfactant driven nanopattern formation on Si substrate in which the Si substrate was eroded with energetic Xenon ions in the presence of a constant flux of Fe atoms acting as a surfactant. Zhang *et al.* proposed that curvature dependent sputtering does not play any role in nanopattern formation rather an uneven sputtering of the surface is a result of different sputtering rates of pure Si and Fe silicide.[35] Recently, the effect of bonding strength of metal silicide formation on the pattern formation has been studied in detail.[36] Zhou *et al.* developed a continuum model to describe the pattern formation at normal incidence with the incorporation of Fe.[37] In which surface stress induced instability competes with the surface relaxation mechanism leading to the observed pattern formation.

[a)]Electronic mail: sarathlal.koyilothvayalil@desy.de

 © 2015 AIP Publishing LLC

[This article is copyrighted as indicated in the article. Reuse of AIP content is subject to the terms at: http://scitation.aip.org/termsconditions. Downloaded to] IP: 131.169.95.181 On: Thu, 22 Jan 2015 12:46:14

According to Shenoy *et al*.[33] and Bradley *et al*.,[34] decomposition or phase separation occurs simultaneously with changes in the surface topography because of the anisotropy in the sputtering rate and the surface diffusivity of the two components. The spontaneously modulated composition can be in-phase or out of-phase with the rippled topography depending upon the erosion parameter.[33] The degree of such kinetic decomposition can be varied by tuning the flux of the ion beam.[33]

A detailed understanding of the atomic level mechanism for nanopattern formation is needed in order to have a better control on the structure of the nanopatterns and to tailor them according to the requirement. In order to differentiate between theoretical models, a study of the evolution of morphology and composition inhomogeneity as a function of ion fluence using advanced characterization techniques is needed. Recently, grazing incidence small angle x-ray scattering (GISAXS) has been used widely to explore *in-situ* and *ex-situ* as an ideal tool for the study of morphological changes during the evolution of surface patterns.[27,38–40] In this work, a comparative analysis of surface evolution with ion fluence using atomic force microscopy (AFM) and GISAXS has been done on Fe assisted ion irradiated samples to provide an insight in to the mechanism at the initial stages of pattern formation.

II. EXPERIMENTAL DETAILS

In our study, single-crystalline Si (100) substrates of size $10 \times 10\,\text{mm}^2$ with measured root mean square surface roughness $\sigma = 0.4\,\text{nm}$ have been used. The substrates were cleaned in an ultrasonic bath with water and acetone sequentially. The irradiation has been performed in a high vacuum chamber equipped with a radio frequency ion source (Veeco RF source), which gave a collimated beam of 3 cm diameter, at a base pressure of 3×10^{-7} mbar. 1 keV Ar ions have been used for erosion. The constant ion flux of 2.4×10^{15} ions cm^{-2} s^{-1} has been used for all the samples. Fluence at the sample was calculated by taking the beam-current value from the power supply and assuming a uniform cross-section of 3 cm diameter for the beam. As a result, there could be a large error in the absolute value of the fluence. However, since the beam current was very stable ($\pm 1\%$), error bar on the relative fluences of different samples was of the same order. Commercially available pure quality (99.99%) sputter targets of Fe of $100\,\text{mm} \times 100\,\text{mm}$ have been used as the source for the metal incorporation. The schematic of the geometry used is shown in Figure 1. One part of the beam irradiated the Si substrate at normal incidence while the other part simultaneously irradiated the Fe target kept at an oblique angle of 45° adjacent to the Si.

Surface morphology of the irradiated samples was analyzed by means of AFM using Digital Instruments (Model-Nanoscope-E) in contact mode. From the AFM images, power spectral density (PSD) functions were extracted using the software Gwyddion.[41] Additionally, Rutherford backscattering spectrometry (RBS) was used to find out the concentration of Fe atoms in the near surface region. The RBS measurements have been performed at IGCAR, Kalpakkam, using a beam of

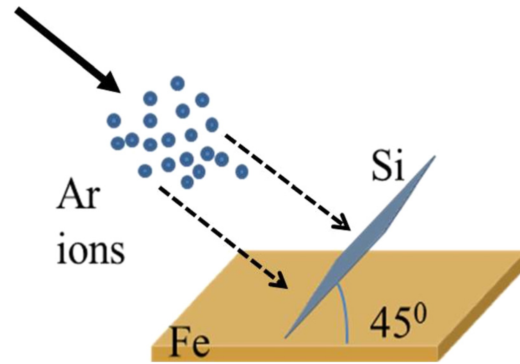

FIG. 1. The schematic sketch of the geometry used for ion beam erosion.

2 MeV He$^+$ ions and the data have been analyzed using SIMNRA code.[42] GISAXS measurements were performed in order to elucidate the morphological changes with varying ion fluence at the sample using a micro beam at MiNaXS/P03 beam line (PETRA III, DESY).[43–45] The energy of the beam used was 11.4 keV with a beam size of $22 \times 18\,\mu\text{m}$. The data have been extracted using the program DPDAK.[46]

III. RESULTS AND DISCUSSIONS

Figures 2(a)–2(f) show the AFM images of Si (100) substrate irradiated at normal incidence with 1 keV Ar ions with simultaneous incorporation of Fe atoms at different ion fluence values. The AFM images have been taken around 2–3 mm from one of the sides of the Si substrate close to the Fe target. Insets show the corresponding FFT images. Evolution of morphology during the irradiation can be seen in Figure 2. At low ion fluence values, up to 4.8×10^{16} ions cm^{-2} a smooth surface with a partially anisotropic structure has been observed. With increasing ion fluence, anisotropy in the structure starts to develop. The well pronounced ripple structure starts to form at or above the ion fluence value of 2.4×10^{17} ions cm^{-2}. In the FFT, the two well separated intense lobes located about the high intensity zero-frequency signal shows the presence of anisotropic rippled surfaces. The direction of the lobes indicates the direction of the ripple wave vector. From the position of the lobes, one can calculate the wavelength of the ripples. The ripple wave vector is found to be oriented along the direction of Fe flow. For more statistical analysis, PSD functions have been calculated. PSD provides the spectrum of spatial frequencies of the surface. Mathematically, it is the square of the fast Fourier transform performed and it can be written as,[47,48]

$$PSD(f_x, f_y) = \lim_{x \to \infty} \frac{1}{L^2} \left| \int_{-\frac{L}{2}}^{\frac{L}{2}} \int_{-\frac{L}{2}}^{\frac{L}{2}} h(x, y) \times \exp[-2\pi i (f_x x + f_y y)] \mathrm{d}x \mathrm{d}y \right|^2, \quad (1)$$

where $h(x, y)$ defines the surface height and f_x and f_y represent the spatial frequencies, and L denotes the length of the scan area. But for anisotropic surfaces one dimensional power spectral density (1D-PSD) is preferred. In our case,

[This article is copyrighted as indicated in the article. Reuse of AIP content is subject to the terms at: http://scitation.aip.org/termsconditions. Downloaded to] IP: 131.169.95.181 On: Thu, 22 Jan 2015 12:46:14

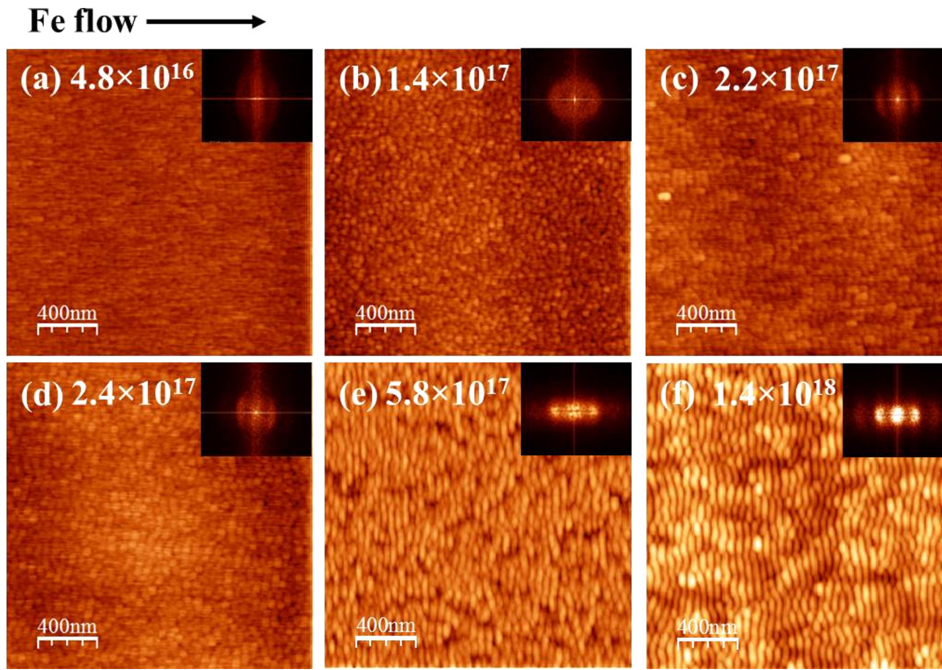

FIG. 2. The AFM images of Si (100) substrate irradiated at normal incidence with 1 keV Ar ions with the simultaneous incorporation of Fe atoms at different ion fluence values ranging from 4.8×10^{16} to 1.4×10^{18} ions cm^{-2}. Corresponding Fourier transform of the images is shown in the inset. Direction of Fe flow for all the samples is indicated in top left.

ID-PSD[41] has been plotted by considering the dominant frequencies in a direction along the ripple wave vector and the corresponding logarithmic plot is shown in Figure 3.

In Figure 3, the large peak in the ID-PSD corresponds to the average wavelength of the ripples. It is clear that at low ion fluence values no pronounced peaks corresponding to the periodic structures are present. Further increase in the ion fluence leads generation of broad peak in the PSD, showing the presence of correlated structures and multiple peaks with a well defined width for higher ion fluence values indicating the presence of ordered structures with large correlation length.

In order to obtain a better information about the concentration of Fe (C_{Fe}), RBS measurements have been done (Figure 4(a)). The RBS spectra reveal the presence of Fe and implanted Ar ions in the surface region (inset of Figure 4(a)). To fit RBS data, we have considered layer with

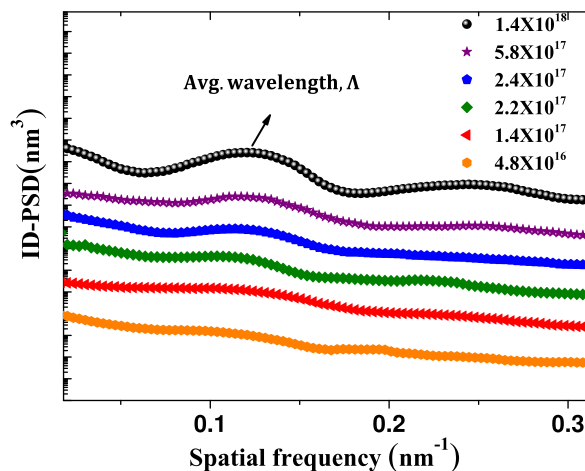

FIG. 3. The 1D-PSD functions of the corresponding AFM images shown in Figure 2 (ion fluence values are in ions. cm^{-2}). For the sake of clarity, the data have been vertically shifted.

different concentrations of Fe and Si. Overall concentration of iron in the surface region as obtained from RBS measurements is 25% for fully developed rippled sample. For the low ion fluence values, the C_{Fe} is initially found to be less, and it increases for further increase in the ion fluence. At around a value of 5.8×10^{17} ions cm^{-2}, the C_{Fe} reaches at a maximum value and saturates for higher fluence. At this region, well ordered ripples were formed (Figure 2). The saturation of the C_{Fe} indicates that Fe atoms lie on the surface. There are also theoretical predictions for the need of critical flux values for the pattern formation.[49] XPS measurements performed on one of the sample irradiated with higher ion fluence (5.8×10^{17} ions cm^{-2}) reveal the formation of iron silicide. The XPS spectrum of a representative sample measured at Fe 2p region is shown in Figure 4(b). A small positive shift of around 0.4 eV from the elemental Fe value has been observed for $2p_{3/2}$ level indicating the presence of iron silicide.[50]

As mentioned earlier, there are many theoretical models on the role of impurities on the pattern formation. Following Zhang *et al.*,[35] initially a thin metal silicide film is formed at the Si surface. As a result of further ion irradiation, phase separation takes place at the surface resulting in metal rich and metal depleted silicide. The Fe rich silicide can form either nanodots or nanoripples, depending upon the angle of incidence of the bombarding ions. Subsequently, a different sputtering rate of Fe rich and Fe depleted regions results in pattern formation at the surface. Zhou *et al.*[36] also suggest that a phase separation occurs at the surface. On the other hand, Bradley *et al.* have further extended his theory to explain the impurity assisted nanopattern formation.[34] According to this theory, nanopattern formation and phase separation should proceed simultaneously. Shenoy *et al.*[33] proposed a model to describe sputtering of alloy surfaces, which describes the evolution of both surface height and composition. All these models strongly predict the major

[This article is copyrighted as indicated in the article. Reuse of AIP content is subject to the terms at: http://scitation.aip.org/termsconditions. Downloaded to] IP: 131.169.95.181 On: Thu, 22 Jan 2015 12:46:14

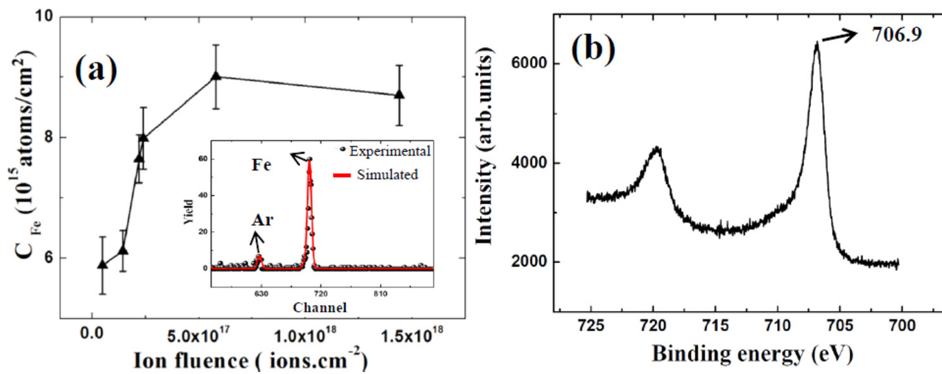

FIG. 4. (a) The variation of concentrations of Fe atoms extracted from RBS data with varying ion fluence and (b) the XPS spectrum measured at Fe 2p region. RBS spectrum of one of the representative sample (higher ion fluence sample) fitted using SIMNRA code is given in inset of (a).

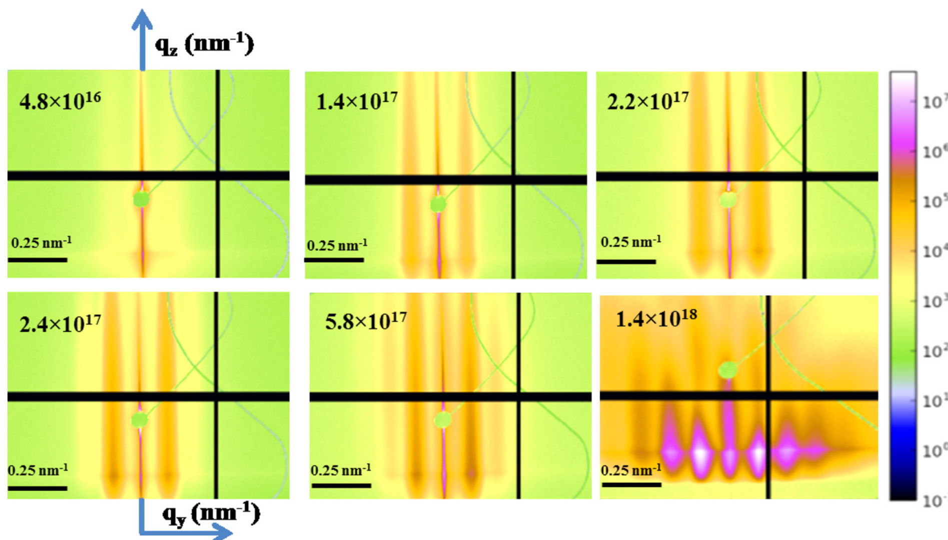

FIG. 5. The 2D-GISAXS images of the Si substrate irradiated in the presence of Fe impurities for different ion fluences (ion fluence values are in ions cm^{-2}).

role of the silicide formation on the pattern formation, but differ in the timescale of silicide formation.

In order to differentiate between models proposed for impurity assisted pattern formation, it is crucial to determine whether phase separation precedes the ripple formation or the two processes occur concurrently. GISAXS is a very suitable method to clarify this point. AFM measurements performed on these samples provided the information about the development of surface topography with the ion fluence. On the other hand, GISAXS measurement will probe the lateral variations of the electron density, so GISAXS will be sensitive to surface topography as well as to any phase separation occurring in the surface region. Figures 5(a)–5(f) show the 2D GISAXS images taken for the same samples. The vertically elongated side peaks observed around the central intense peak are due to the periodic and correlated nature of the samples. One can calculate the real space distance between the correlated structures using the expression, $\Lambda = 2\pi/q_y$. The corresponding line profiles along q_y direction for a fixed q_z value corresponding to the Yoneda region[51] (maximum scattering intensity region when the scattering angle of the scattered beam is close to critical angle) for all samples are shown in Figure 6. The width of the peak is narrowed with increasing ion fluence values, which shows the formation of highly correlated structures. Slight difference in the intensities of the side peaks for positive and negative q_y values is due to the asymmetric nature of the pattern.[52] The lack of broadening around the intense center peak for low ion fluence values indicates the absence of any kind of formation of large scale corrugations in a direction along the ripple wave vector as predicted.[53,54] One can see the

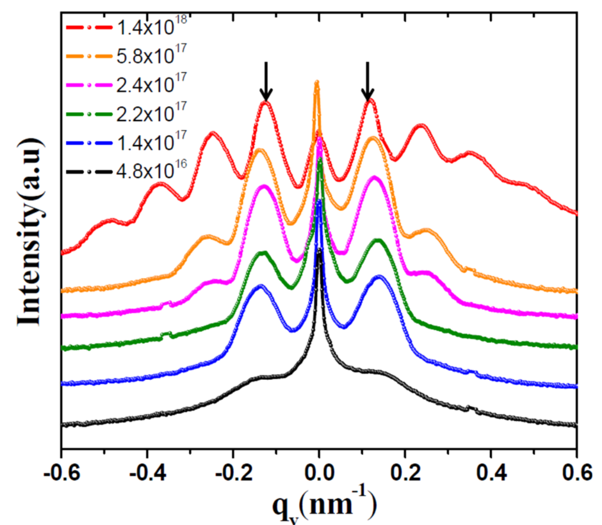

FIG. 6. The line profiles along q_y of GISAXS taken at fixed q_z (Si yoneda) for different ion fluence values (ion fluence values are in ions cm^{-2}). For the sake of clarity, the data have been vertically shifted.

[This article is copyrighted as indicated in the article. Reuse of AIP content is subject to the terms at: http://scitation.aip.org/termsconditions. Downloaded to] IP: 131.169.95.181 On: Thu, 22 Jan 2015 12:46:14

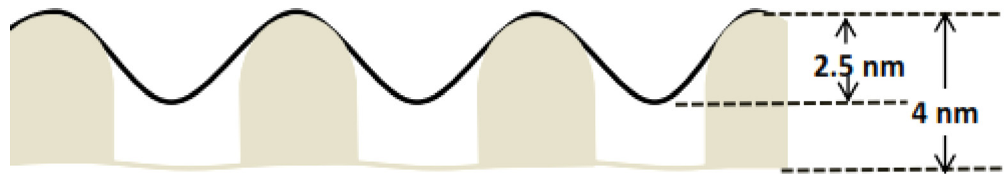

FIG. 7. Schematic of the surface region with fully developed ripple structure and complete phase separation.

broadening around the center peak for higher fluence values. This indicates the formation of large scale structures of the order of a few hundreds of nanometers along with the ripple structures. One can see that, as the ripple structure develops, the intensity of the sidebands at q_y values corresponding to the ripple wavelength increases indicating the growth of the ripples and increased ordering of the samples.

In general, GISAXS intensity depends upon many factors like wavelength of the x-rays, angle of incidence of the x-ray on the sample, etc. In the present case, since from sample to sample all the factors are kept identical, the intensity of the sidebands will be proportional to the electron density contrast in a direction normal to the direction of x-ray propagation. Furthermore, close to the critical angle of incidence, the penetration depth of x-rays in the sample is around 4 nm. Therefore, the intensity of sidebands will depend up on the electron density contrast averaged over a depth of 4 nm. The electron density contrast can develop due to phase separation in the surface region, or due to formation of ripples or due to both of them. A rough estimate of the electron density contrast due to the above factors can be made as follows: (i) From the analysis of RBS data, one finds that Fe is present up to a depth of 5.5 nm, and in this region overall Fe concentration is 25 at. %. If one assumes a perfect phase separation in the surface region, the two regions will consist of pure Si and Si-50 at. %Fe. Accordingly, the electron densities of the two regions are 6.92×10^{23} electrons cm^{-3} and 1.52×10^{24} electrons cm^{-3} and thus a contrast of 55%. (ii) In case ripple formation accompanies the phase separation, the two regions will consist of air and Si-50 at. %Fe. Thus, in fully developed ripple structure which has a modulation depth of 2.5 nm, electron density contrast will be 100%. Below this depth, the contrast will be only due to phase separation (Figure 7). Therefore, electron density contrast averaged over penetration depth of x-rays (4 nm) will be ~83%. Thus, the electron density contrast in the two cases is comparable, and intensity of side-bands is equally sensitive to the two possibilities. On the other hand, AFM gives only information about the ripple formation. Thus, the two techniques together can differentiate between the above two possibilities.

Figure 8 gives the height of the sidebands in the GISAXS patterns as a function of ion fluence. For a comparison, the intensity of the side bands as obtained from the power spectral density of AFM patterns is also plotted. While the intensity of the peak in the PSD of the AFM will be proportional to the amplitude of the surface ripples only, the intensity of the sidebands in GISAXS depends upon height of the ripples as well as any phase separation in the iron silicide layer in the surface. In Figure 8, one can see that the fluence dependence of both intensities is identical. Comparative AFM and GISAXS (at ELETTRA, Italy) measurements performed on another set of similar samples also got the similar behavior (Figure 9). This provides clear evidence that phase separation does not precede the ripple formation rather it concurrently develops along with the ripple structure. This observation contradicts some model where phase separation is expected to occur first and subsequently due to the variation in Fe concentration, ripple patterns develops. Present work supports the models proposed by Bradley *et al.*[34] and Shenoy *et al.*[33] where phase separation and ripple formation occur concurrently.

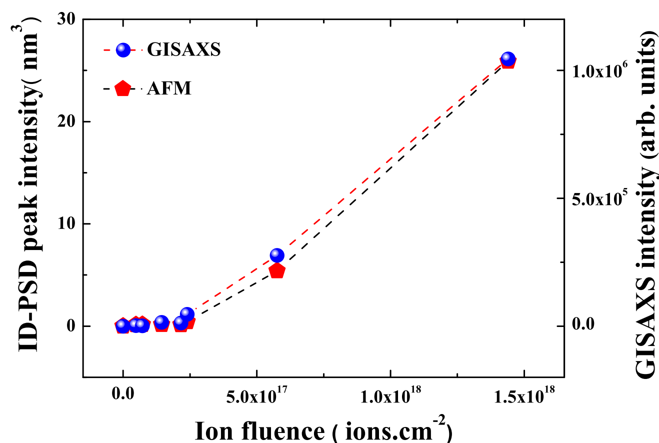

FIG. 8. Comparison of intensity of first order sidebands in both 1D-PSD of AFM and GISAXS for different ion fluences.

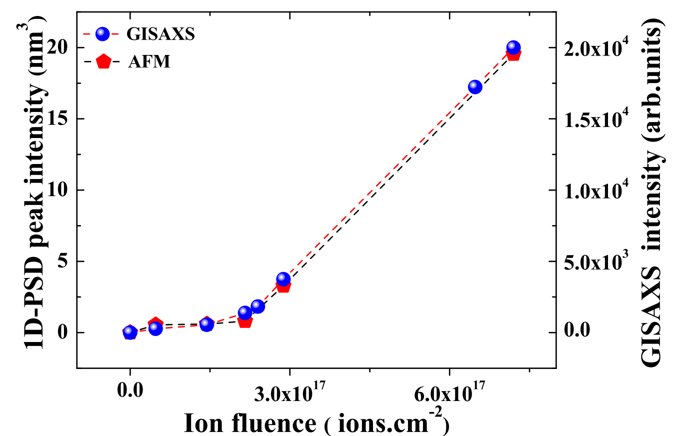

FIG. 9. A comparison of intensity of first order sidebands in both 1D-PSD of AFM and GISAXS for different ion fluences for the similar set of samples prepared separately. GISAXS measurements have been carried out at SAXS beamline Elettra, Trieste.

[This article is copyrighted as indicated in the article. Reuse of AIP content is subject to the terms at: http://scitation.aip.org/termsconditions. Downloaded to] IP: 131.169.95.181 On: Thu, 22 Jan 2015 12:46:14

IV. CONCLUSION

In summary, the well-ordered nanorippled Si substrates have been prepared by normal incidence ion beam sputtering with simultaneous incorporation of Fe atoms. Ordering of the nanoripples is found to be increasing with increasing values of ion fluence. Comparative analysis of AFM and GISAXS has shown that phase separation of the metal silicide formed during the erosion does not precede the ripple formation rather it concurrently develops along with the ripple structure. Our experimental observations can provide an insight for the future theoretical developments, which should consider the very early developmental stages of pattern formation in details.

ACKNOWLEDGMENTS

Thankful to Mr. Mohan Gangarade, UGC-DAE CSR, Indore, India, for AFM measurements and Dr. B. K. Panigrahi, Dr. S. Balaji, IGCAR, Kalpakkam, India, for RBS measurements. Dr. Sigrid Bernstorff, Elettra, Trieste, Italy, for the preliminary GISAXS measurements.

[1]S. Facsko, T. Dekorsy, C. Koerdt, C. Trappe, H. Kurz, A. Vogt, and H. L. Hartnagel, Science **285**, 1551 (1999).
[2]U. Valbusa, C. Boragno, and F. Buatier de Mongeot, J. Phys.: Condens. Matter. **14**, 8153 (2002).
[3]J. Erlebacher, M. J. Aziz, M. E. Chason, M. B. Sinclair, and J. A. Floro, Phys. Rev. Lett. **82**, 2330 (1999).
[4]F. Frost, A. Schindler, and F. Bigl, Phys. Rev. Lett. **85**, 4116 (2000).
[5]B. Ziberi, F. Frost, Th. Höche, and B. Rauschenbach, Appl. Phys. Lett. **87**, 033113 (2005).
[6]F. Frost and B. Rauschenbach, Appl. Phys. A: Mater. Sci. Process **77**, 1 (2003).
[7]B. Ziberi, F. Frost, Th. Höche, and B. Rauschenbach, Phys. Rev. B **72**, 235310 (2005).
[8]K. V. Sarathlal, S. Potdar, M. Gangrade, V. Ganesan, and A. Gupta, Adv. Mater. Lett. **4**, 398 (2013).
[9]K. V. Sarathlal, D. Kumar, and A. Gupta, Appl. Phys. Lett. **98**, 123111 (2011).
[10]K. V. Sarathlal, D. Kumar, V. Ganesan, and A. Gupta, Appl. Surf. Sci. **258**, 4116 (2012).
[11]J. Fassbender, T. Strache, M. O. Liedke, D. Markó, S. Wintz, K. Lenz, A. Keller, S. Facsko, I. Mönch, and J. McCord, New. J. Phys. **11**, 125002 (2009).
[12]M. Körner, K. Lenz, M. O. Liedke, T. Strache, A. Mücklich, A. Keller, S. Facsko, and J. Fassbender, Phys. Rev. B **80**, 214401 (2009).
[13]M. O. Liedke, B. Liedke, A. Keller, B. Hillebrands, A. Mücklich, S. Facsko, and J. Fassbender, Phys. Rev. B **75**, 220407(R) (2007).
[14]G. Agnus, T. Maroutian, A. Fleurence, B. Bartenlian, M. Hanbucken, and P. Beauvillain, Appl. Phys. Lett. **103**, 123117 (2013).
[15]K. Chen, R. Frömter, S. Rössler, N. Mikuszeit, and H. P. Oepen, Phys. Rev. B **86**, 064432 (2012).
[16]M. O. Liedke, M. Körner, K. Lenz, F. Grossmann, S. Facsko, and J. Fassbender, Appl. Phys. Lett **100**, 242405 (2012).
[17]S. Camelio, D. Babonneau, D. Lantiat, L. Simonot, and F. Pailloux, Phys. Rev. B **80**, 155434 (2009).
[18]R. M. Bradley and J. M. Harper, J. Vac. Sci. Technol. A **6**, 2390 (1988).
[19]R. Cuerno and A.-L. Barabási, Phys. Rev. Lett. **74**, 4746 (1995).
[20]J. Muñoz-García, M. Castro, and R. Cuerno, Phys. Rev. Lett. **96**, 086101 (2006).
[21]M. A. Makeev, R. Cuerno, and A.-L. Barabási, Nucl. Instrum. Methods Phys. Res. B **197**, 185 (2002).
[22]C. S. Madi, E. Anzenberg, K. F. Ludwig, Jr., and M. J. Aziz, Phys. Rev. Lett. **106**, 066101 (2011).
[23]T. Kumar, A. Kumar, D. C. Agarwal, N. P. Lalla, and D. Kanjilal, Nanoscale. Res. Lett. **8**, 336 (2013).
[24]G. Carter, V. Vishnyakov, Yu. V. Martynenko, and M. J. Nobes, J. Appl. Phys. **78**, 3559 (1995).
[25]G. Carter and V. Vishnyakov, Phys. Rev. B **54**, 17647 (1996).
[26]R. Gago, L. Vázquez, R. Cuerno, M. Varela, C. Ballesteros, and J. M. Albella, Appl. Phys. Lett. **78**, 3316 (2001).
[27]G. Ozaydin, A. Ozcan, Y. Wang, K. F. Ludwig, Jr., H. Zhou, R. Headrick, and P. Siddons, Appl. Phys. Lett. **87**, 163104 (2005).
[28]C. S. Madi and M. J. Aziz, Appl. Surf. Sci. **258**, 4112 (2012).
[29]G. Ozaydin, K. F. Ludwig, Jr., H. Zhou, and R. L. Headrick, J. Vac. Sci. Technol B **26**, 551 (2008).
[30]S. Macko, F. Frost, B. Ziberi, D. F. Frster, and T. Michely, Nanotechnology **21**, 085301 (2010).
[31]H. Hofsäss and K. Zhang, Appl. Phys. A **92**(3), 517 (2008).
[32]J. A. Sánchez-García, L. Vázquez, R. Gago, A. Redondo-Cubero, J. M. Albella, and Z. Czigány, Nanotechnology **19**, 355306 (2008).
[33]V. B. Shenoy, W. L. Chan, and E. Chason, Phys. Rev. Lett. **98**, 256101 (2007).
[34]R. M. Bradley and P. D. Shipman, Phys. Rev. Lett. **105**, 145501 (2010).
[35]K. Zhang, M. Brötzmann, and H. Hofsäss, New. J. Phys. **13**, 013033 (2011).
[36]O. El-Atwani, S. Gonderman, A. DeMasi, A. Suslova, J. Fowler, M. El-Atwani, K. Ludwig, and J. P. Allain, J. Appl. Phys. **113**, 124305 (2013).
[37]J. Zhou and M. Lu, Phys. Rev. B **82**, 125404 (2010).
[38]D. Babonneau, S. Camelio, E. Vandenheck, S. Rousselet, M. Garel, F. Pailloux, and P. Boesecke, Phys. Rev. B **85**, 235415 (2012).
[39]A. Buffet, M. M. Abul Kashem, K. Schlage, S. Couet, R. Rohlsberger, A. Rothkirch, G. Herzog, E. Metwalli, R. Meier, G. Kaune, M. Rawolle, P. Müller-Buschbaum, R. Gehrke, and S. V. Roth, Langmuir **27**(1), 343 (2011).
[40]P. Müller-Buschbaum, Anal. Bioanal. Chem. **376**, 3 (2003).
[41]D. Nečas and P. Klapetek, Cent. Eur. J. Phys. **10**(1), 181 (2012); P. Klapetek, D. Nečas, and C. Anderson, Gwyddion user guide, see http://gwyddion.net/documentation/ (2009).
[42]M. Mayer, SIMNRA Users Guide, Report IPP 9/113, Max-Planck-Institut für Plasmaphysik, Garching, Germany (1997).
[43]A. Buffet, A. Rothkirch, R. Dohrmann, V. Körstgens, M. M. A. Kashem, J. Perlich, G. Herzog, M. Schwartzkopf, R. Gehrke, P. Müller-Buschbaum, and S. V. Roth, J. Synchr. Radiation **19**, 647–653 (2012).
[44]S. V. Roth, G. Herzog, V. Körstgens, A. Buffet, M. Schwartzkopf, J. Perlich, M. M. Abul Kashem, R. Döhrmann, R. Gehrke, A. Rothkirch, K. Stassig, W. Wurth, G. Benecke, C. Li, P. Fratzl, M. Rawolle, and P. Müller-Buschbaum, J. Phys.: Condens. Matter. **23**, 254208 (2011).
[45]G. Santoro, A. Buffet, R. Döhrmann, S. Yu, V. Körstgens, P. Müller-Buschbaum, U. Gedde, M. Hedenqvist, and S. V. Roth, Rev. Sci. Instrum. **85**, 043901 (2014).
[46]G. Benecke, see https://dpdak.desy.de/index.php/Hauptseite (2013).
[47]J. M. Elson and J. M. Bennet, Appl. Opt. **34**, 201 (1995).
[48]A. Duparré, J. Ferre-Borrull, S. Gliech, G. Notni, J. Steinert, and J. M. Bennett, Appl. Opt. **41**, 154 (2002).
[49]R. M. Bradley, Phys. Rev. B **83**, 195410 (2011).
[50]N. Ohtsua, M. Okub, K. Satohb, and K. Wagatsuma, Appl. Surf. Sci. **264**, 219 (2013).
[51]Y. Yoneda, Phys. Rev. B **131**, 2010 (1963).
[52]D. Carbone, A. Alija, O. Plantevin, R. Gago, S. Facsko, and T. H. Metzger, Nanotechnology **19**, 035304 (2008).
[53]A. Keller, S. Robach, S. Facsko, and W. Moller, Nanotechnology **19**, 135303 (2008).
[54]P. F. A. Alkemade and Z. X. Jiang, J. Vac. Sci. Technol. B **19**, 1699 (2001).

[This article is copyrighted as indicated in the article. Reuse of AIP content is subject to the terms at: http://scitation.aip.org/termsconditions. Downloaded to] IP: 131.169.95.181 On: Thu, 22 Jan 2015 12:46:14